RSC Advances

PAPER

View Article Online
View Journal | View Issue

Cite this: *RSC Adv.*, 2023, **13**, 22017

Bifunctional CuS/Cl-terminated greener MXene electrocatalyst for efficient hydrogen production by water splitting

Bilal Sarfraz,[a] Muhammad Taqi Mehran, *[a] Faisal Shahzad, [b] Sajjad Hussain,[c] Salman Raza Naqvi,[a] Hassnain Abbas Khan [d] and Khalid Mahmood *[e]

Metal sulfides and 2D materials are the propitious candidates for numerous electrochemical applications, due to their superior conductivity and ample active sites. Herein, CuS nanoparticles were fabricated on 2D greener HF-free Cl-terminated MXene ($Ti_3C_2Cl_2$) sheets by the hydrothermal process as a proficient electrocatalyst for the hydrogen evolution reaction (HER) and overall water splitting. CuS/$Ti_3C_2Cl_2$ showed an overpotential of 163 mV and a Tafel slope of 77 mV dec^{-1} at 10 mA cm^{-2} for the HER. In the case of the OER, CuS/$Ti_3C_2Cl_2$ exhibited an overpotential of 334 mV at 50 mA cm^{-2} and a Tafel slope of 42 mV dec^{-1}. Moreover, the assembled CuS/$Ti_3C_2Cl_2$||CuS/$Ti_3C_2Cl_2$ electrolyzer delivered current density of 20 mA cm^{-2} at 1.87 V for overall water splitting. The CuS/$Ti_3C_2Cl_2$ electrocatalyst showed excellent stability to retain 96% of its initial value for about 48 hours at 100 mA cm^{-2} current density. The synthesis of CuS/$Ti_3C_2Cl_2$ enriches the applications of MXene/metal sulfides in efficient bifunctional electrocatalysis for alkaline water splitting.

Received 18th April 2023
Accepted 9th July 2023

DOI: 10.1039/d3ra02581k

rsc.li/rsc-advances

1 Introduction

To surmount the increasing energy demand and the incremental fossil fuel depletion, high-performance energy storage devices *e.g.* supercapacitors and batteries, over alternative energy sources including nuclear, solar and wind energy, are required.[1–3] The researchers have dedicated significant attention to the development and design of new eco-friendly materials for energy storage devices and electrochemical energy production. In contrast, the hydrogen evolution reaction (HER) is a significantly proficient way to produce green energy. To attain a specific current density, the potent electrocatalysts for HER produce low overpotentials and increase the rate of electrolysis.[4–7] Platinum is the most efficient electrocatalyst for hydrogen evolution reactions (HER), but its low stability towards impurities and high cost hinder its use as a commercial electrocatalyst.[8–11]

Extensive research has been going on two-dimensional (2D) materials owing to their electronic,[12,13] optical,[14] mechanical,[15] and structural properties.[16–18] Except for graphene, phosphorene, transition metals dichalcogenides (TMDs), and their derivatives are examples of the ultimate analyzed two-dimensional (2D) materials. In 2011, the first member of the MXene family (synthesized from MAX phase), titanium carbide (Ti_3C_2) was introduced, having exclusive electronic and structural features, facilitating their usage on several applications.[19–21] Generally, the MAX phase is the starting compound, and MXenes are manufactured by explicitly etching the A element layers from the MAX phase by using F-containing acids/salts such as HF, NH_4HF_2, or LiF/HCl, where A indicates Al or Si.[22,23] MXenes prepared by HF acid has its own demerits; HF breaks the MXene sheets,[24] being such a strong acid causes several health and environmental issues.[25] So, HF-free MXenes can play a better role than ordinary HF-based MXenes.

Recently, metal sulfides, nitride, phosphates have drawn vast attention because of reversible charge/discharge properties and ample redox reactions in contrast with corresponding oxides.[26,27] Moreover, binary metal sulfides and mixed metals sulfides, like NiS, CuS, CoS, Ni_2S, and $NiCo_2S_4$ along with other 3D and 2D materials (MXenes, graphene, *etc.*) in the form of composites are used in enormous applications like electrocatalysts for overall water splitting reactions and electrode material for supercapacitors.[28,29] Recently a review on the transition metal chalcogenides shows that metal sulfides alone did not show much good results, but when these materials are deposited on 2D nanosheets like MXenes or graphene

[a]*School of Chemical and Materials Engineering (SCME), National University of Sciences and Technology (NUST), H-12 Campus, Islamabad 44000, Pakistan. E-mail: taqimehran@scme.nust.edu.pk*

[b]*Department of Metallurgy and Materials Engineering, Pakistan Institute of Engineering and Applied Sciences (PIEAS), Islamabad 45650, Pakistan*

[c]*Department of Nanotechnology and Advanced Materials Engineering, Sejong University, Seoul, 05006, Republic of Korea*

[d]*Clean Combustion Research Center, King Abdullah University of Science and Technology, Thuwal 23955-6900, Kingdom of Saudi Arabia*

[e]*Department of Chemical & Polymer Engineering, University of Engineering & Technology Lahore, Faisalabad Campus, Khurrianwala, Faisalabad, Pakistan. E-mail: khalid@uet.edu.pk*

electrochemical activities improved in a greater extend because both the surface area and conductivity increases.[30] Among the most striking transition-metal chalcogenides, copper sulfide (CuS) is extensively studied as a secondary material in electrochemical sensors,[31] Li-ion batteries,[32,33] and solar cells applications[34,35] due to its metal-like conductivity, inexpensive and plentiful qualities. Recently,[36] the composite of CuS nanomaterial with two-dimensional (2D) nano MXene (HF acid-based) was investigated for supercapacitor applications. MXene provided more surface area which reduced the diffusion resistance and enabled transmission of an electron, hence gained high capacity, while CuS particles as semiconductor material increased the overall conductivity of the composite.[36]

In this study, CuS/$Ti_3C_2Cl_2$ composite was synthesized by hydrothermal deposition of copper sulfide (CuS) on Cl-terminated HF-free MXene ($Ti_3C_2Cl_2$) sheets. CuS nanoparticles decoration on the Cl-terminated MXene sheets increased the interlayer spacing and provided more surface area for electrochemical activity. CuS nanoparticles having metal like conductive behavior, not only provided the additional surface area for reaction but also improved the overall conductivity of the composite. The CuS/$Ti_3C_2Cl_2$ exhibited enhanced electrochemical activities for HER and OWS. The overpotential of 163 mV to get 10 mA cm^{-2} current density for HER and incase of overall water splitting the composite showed the potential of 1.87 V to get 10 mA cm^{-2} current density in CuS/$Ti_3C_2Cl_2$||CuS/$Ti_3C_2Cl_2$ two electrode system. The composite appeared to be a great addition in the library of bifunctional electrocatalysts for overall water splitting applications.

2 Experimental section

2.1 Materials

For the synthesis of HF-MXene, Cl-terminated MXene, and CuS/Cl-terminated MXene, the materials used were MAX phase powder (Ti_3AlC_2) with the particle size less than 40 μm, 37% HCl, 40% HF, copper chloride ($CuCl_2$), ethylene glycol $(CH_2OH)_2$, copper nitrate ($Cu(NO_3)_2$), thioacetamide (CH_3CSNH_2), absolute ethanol and deionized water.

2.2 Synthesis of HF MXene

The MXene ($Ti_3C_2T_x$) was prepared from the MAX phase (Ti_3AlC_2) with HF acid treatment. 10 mL of 50% HF acid was dropped into 10 mL of deionized water in a pp bottle. 2 grams of MAX phase powder was added slowly to into the HF solution under magnetic stirring. After adding the MAX phase, the heating was started. The temperature of the solution was maintained at 35–40 °C. The reaction time under this temperature was 8 h with continuous stirring. After the reaction, reacted solution was cool to room temperature. The reacted mixture was washed with deionized water with the help of a centrifuge at 4000 rpm for 2 h with several cycles of washing (time per cycle 5 minutes). After maintaining pH $\geq$ 6, the mixture was finally washed with ethanol. The mixture was dried for overnight drying at 80 °C in a vacuum oven.

2.3 Synthesis of Cl-terminated MXene

Greener Cl-terminated MXene was prepared using MAX phase and copper chloride at 550 °C for 5–6 h in a tube furnace under an inert Ar gas environment by the thermal treatment process. Copper chloride and MAX phase were mixed in a vacuum glove box under Ar with a molar ratio of 6 : 1. Then mixed powder was shifted into a boat crucible and placed in a tube furnace. The reacted mixture was treated with 2% HCl for about 2 h under magnetic stirring for the removal of residues. The product was separated by centrifuge, with several washes with DI water to maintain a pH of around 6. Finally, the prepared Cl-terminated MXene was rinsed with absolute ethanol and dried in the oven at 80 °C for 24 hours.

2.4 Synthesis of CuS/Cl-terminated MXene

The CuS/Cl-terminated MXene composite was fabricated by using a hydrothermal process. 200 mg of Cl-MXene powder and 300 mg of copper nitrate were added into 60 mL of ethylene glycol and magnetically stirred for 30–40 min. The 300 mg of thioacetamide was dropped slowly into the solution. After making the perfect suspension, a solution was transferred into a Teflon cup and placed into an autoclave. The reaction was carried out for 9 h at 150 °C. Then the reacted product was received by centrifuge and rinsed with DI water several times at 4500 rpm and finally with ethanol. The product was dried overnight at 85 °C.

2.5 Synthesis of HF-MXene, Cl-MXene, and CuS/Cl-MXene electrodes

The electrodes for characterization purposes were prepared on Ni foam (as substrate). Firstly, a 1 × 1 cm^2 piece of nickel foam was treated with 3 M HCl acid solution to eliminate the oxide layers and then dried at 60 °C for 4 hours. The WE (working electrode) were prepared by loading synthesized materials ink. For the ink preparation 500 μL of deionized water was taken in a glass vial. 450 μL isopropyl alcohol, 50 μL Nafion, and 10 mg of required material were added to that vial. The solution was sonicated for about an hour at room temperature. Then 200 μL of prepared ink suspension was deposited on Ni foam and dried at 60 °C for 3–4 hours.

2.6 Characterization of synthesized materials (HF-MXene, Cl-MXene and CuS/Cl-MXene)

The structural analysis of Cl-terminated MXene was performed by scanning electron microscopy (SEM) (JEOL139/JSM-6490A) equipped with energy-dispersive X-ray spectroscopy (EDX). XRD peaks were obtained by X-ray diffraction (XRD) (STOE-Seifert/X'Pert PRO), using Cu-Kα radiation at 2θ angle values from 5° to 60°. For the chlorine termination, Fourier transforms infrared spectroscopy (FTIR) (iS50 FT-IR spectrometer/Thermo Scientific) was used.

2.7 Electrochemical characterizations of HF-MXene, Cl-MXene and CuS/Cl-MXene

Three electrode system was used for the electrochemical characterization of synthesized materials. Pt mesh was used as

a counter electrode, while Ag/AgCl was as a reference electrode. The working electrode was a 1 cm × 1 cm piece of treated nickel foam with synthesized materials coated on it. Cyclovoltammetry analysis was carried out from 0 to 0.6 V and LSV analysis was conducted for the overall water splitting at 10 mV s^{-1} scan rate, OER was conducted between 1.2 to 1.8 V, while HER was in the range of −0.5 to 0 V. The V_{RHE} potential values were calculated by the Nernst equation.

$$V_{RHE} = V_{Ag/AgCl} + 0.059 \times pH + V^{o}_{Ag/AgCl}$$

where V_{RHE} is the value of potential (V) *vs.* RHE, $V_{Ag/AgCl}$ represents the measured potential *vs.* Ag/AgCl value, and the value of $V^{o}_{Ag/AgCl}$ is 0.198 V at 25 °C. For iR corrections of all measurements, the value of R_s (series resistance) was calculated from electrochemical impedance spectroscopy (EIS). Electrochemical impedance spectroscopy was carried at 10 mV sinusoidal amplitude out in the frequency range of 100 mHz to 1 MHz.

3 Results and discussion

3.1 Material characterization of synthesized electrocatalyst catalysts

The evolution of CuS/Cl-terminated MXene from MAX phase is illustrated with the help of schematic diagram in Fig. 1. Fig. 1 shows that 3D MAX phase was thermally treated with Lewis salts to etch the aluminum metal layer to make it 2D sheet like structure. Further the activity of that 2D Cl-terminated MXene was enhanced by depositing the CuS particles on these 2D Cl-terminated sheets by a hydrothermal process. To confirm the morphology and microstructure of Cl-terminated Mxene ($Ti_3C_2Cl_2$) and copper sulfide/Cl-terminated MXene (CuS/$Ti_3C_2Cl_2$), SEM analysis was performed. Fig. 2(a) shows the three-dimensional (3D) MAX phase material (Ti_3AlC_2) from which the MXene is synthesized. In Fig. 2(b) the layered sandwich-like structure confirms the formation of two-dimensional (2D) Cl-terminated MXene.[37,38] Fig. 2(c) and (d) exhibit the SEM images of CuS/$Ti_3C_2Cl_2$, where CuS nanoparticles are deposited on the Cl-terminated MXene sheets. A large number of CuS particles are dispersed on the surface and interlayer space of Cl-terminated MXene sheets, preventing the collapse and stacking of Cl-MXene sheets.[36]

To further examine the formation of Cl-terminated MXene and composite of Cl-MXene with CuS, EDX analysis was carried out. EDX analysis of the prepared composite CuS/$Ti_3C_2Cl_2$ was also performed. Fig. 2(e) shows weight percentages of all the present elements in prepared CuS/Cl-terminated MXene composite. CuS is successfully deposited on the MXene sheet, a plentiful amount of Cu and S is present in the pie chart, confirming the maximum deposition of the CuS on the Cl-terminated MXene. Fig. 2(f) is the corresponding SEM image for elemental mapping. Elemental mapping of all the elements in CuS/$Ti_3C_2Cl_2$ is shown in Fig. 2(g)–(m) to validate the equal sharing of elements. Fig. 3 shows the elemental composition of the synthesized Cl-MXene, it is seen that amount of Al is much reduced as compared to other elements showing the plentiful etching of Al metals to form Cl-MXene. The presence of Cl in Fig. 3 confirms the Cl-termination. Additionally, elemental mapping is provided to validate the equal sharing of elements in the compound.

Fig. 4(a) shows the details of X-ray diffraction (XRD) analysis from base material MAX phase (Ti_3AlC_2) to copper sulfide composite with Cl-terminated MXene (CuS/$Ti_3C_2Cl_2$). (002) peak at 9.4°, (004), (101), (104), (105), (107), (108) and (109) peaks at 19°, 33.95°, 38.95°, 41.75°, 48.4°, 52.35° and 56.35° scan angles

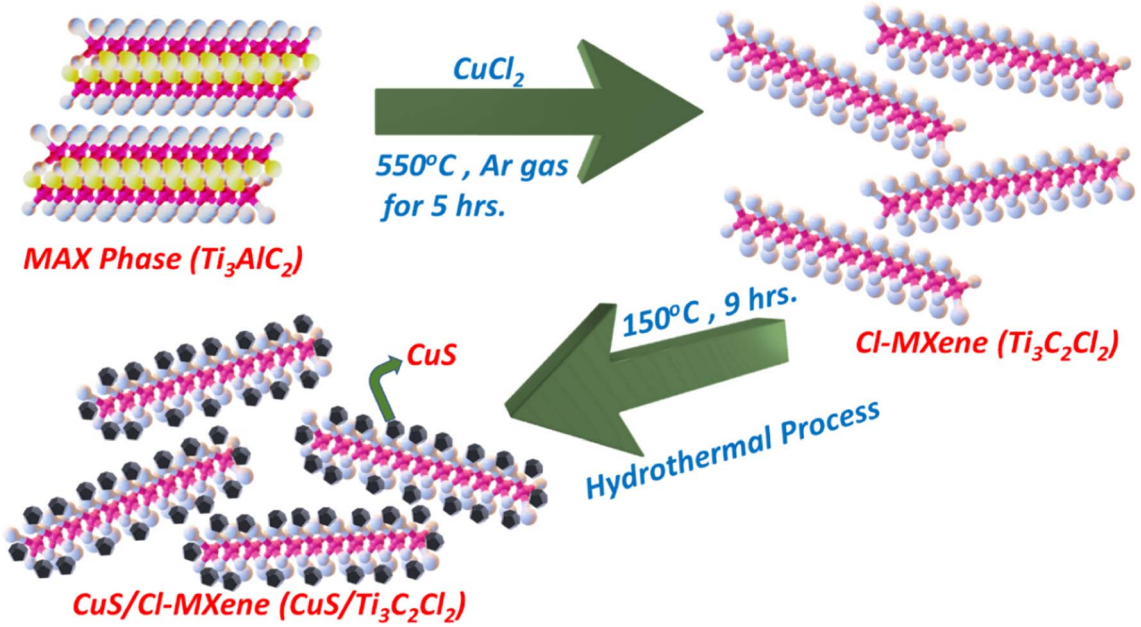

Fig. 1 Schematic illustration of the synthesis of Cl-terminated MXene from the heat treatment procedure of MAX phase (Ti_3AlC_2) and copper chloride ($CuCl_2$), then deposition of CuS nano particles on Cl-MXene sheets by hydrothermal process.

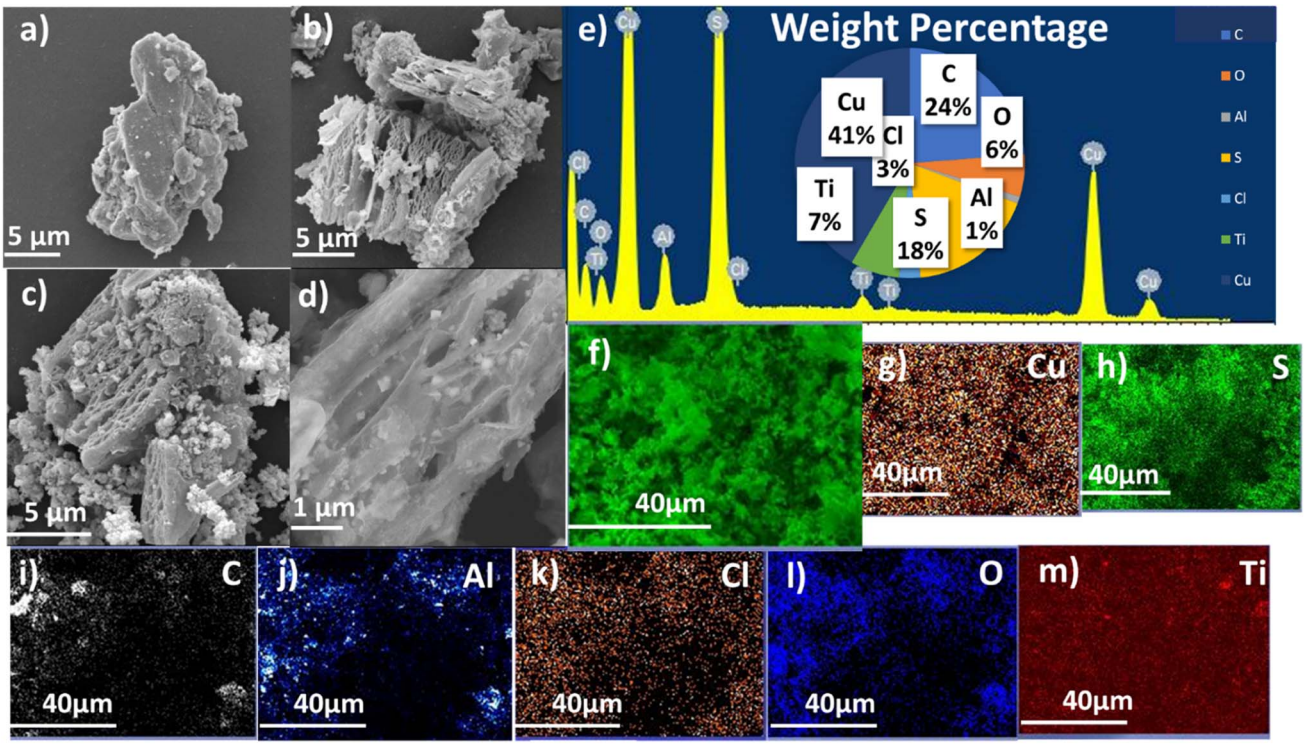

Fig. 2 (a) SEM analysis of three-dimensional (3D) MAX phase (Ti_3AlC_2) material, (b) figure depicts the formation of 2D layer structure of Cl-terminated MXene ($Ti_3C_2Cl_2$), (c) and (d) SEM images of CuS/$Ti_3C_2Cl_2$ composite shows the deposition of CuS particles on Cl-terminated MXene ($Ti_3C_2Cl_2$) sheets, (e) EDX analysis of prepared CuS/$Ti_3C_2Cl_2$ composite together with weight percentage of all the elements present in composite, (f) corresponding SEM image for elemental mapping, (g)–(m) elemental mapping of the elements of prepared CuS/$Ti_3C_2Cl_2$ composite.

related to the planes of MAX phase (Ti_3AlC_2).[39] Hydrofluoric acid (HF) MXene (blue) (Ti_3C_2) peaks (002), (004), and (006) were observed at scan angles 9.1°, 18.42°, and 27.74° respectively.[40] The formation of Cl-terminated MXene was confirmed by the diffraction peaks at 15.45°, 16.2°, 22.95°, 30.9°, 32.25°, and 40.7°, which correspond to the Cl-MXene ($Ti_3C_2Cl_2$).[37,38] In Cl-terminated MXene, the intensity of broadened peaks (002), (004), and (006) were reduced and (002) peak shifted from 9.1° to 7.5°, (004) and (006) peaks shifted from 18.42°, 27.74° to 17.55°, and 27.7° respectively, indicating the increase in inter-layer distance (Bragg diffraction equation).[37,40] The XRD pattern of pure CuS nanoparticles is consistent with the hexagonal structured CuS particles with JCPDS No. 06-0464,[36] the CuS peaks appeared at 28.03°, 29.76°, 32.41°, 42°, 52° and 55.05°. XRD results of CuS/$Ti_3C_2Cl_2$ composite confirm the presence of both Cl-MXene and CuS, as peaks appeared at 16.25°, 27.65°, 31.05° and 32.75° belongs to Cl-MXene($Ti_3C_2Cl_2$). The intensity of these peaks is low due to the excessive CuS deposition. The successful decoration of copper sulfide particles on Cl-terminated MXene was confirmed by XRD of the CuS/$Ti_3C_2Cl_2$ composite, all diffraction peaks at 29.15°, 31.8°, 47.8°, 52.6°, and 59.2° are consistent with the hexagonal structured CuS particles (with JCPDS No. 06-0464).[36]

Fourier transform infrared spectroscopy commonly known as FTIR was used for the molecular fingerprinting of the synthesized materials. Fig. 4(b) shows the detailed analysis of the materials ranging from 0 to 4000 cm^{-1} wavelength. The peaks that appeared at 826 cm^{-1} in Cl-terminated MXene ($Ti_3C_2Cl_2$) and 808 cm^{-1} in CuS/$Ti_3C_2Cl_2$ are the confirmation of C–Cl bond vibration, which be found in Cl-terminated MXene. The band at 3422 cm^{-1} indicates the OH group due to the existence of absorbed water.[41] While the characteristic band at 2916 cm^{-1} may correspond to the N–H stretching, which comes from one of the raw materials (thioacetamide) used to prepare copper sulfide (CuS) on Cl-terminated MXene sheets. A peak at 1623 cm^{-1} corresponds to C=O, while a 1072 cm^{-1} peak is related to either C–O or S–O.[42] C–O may come from ethanol, which was used for the washing of the prepared catalyst.[41] The peak at 602 cm^{-1} indicates the vibrational mode of the Cu–S bond,[41–44] which confirms the formation of CuS on Cl-terminated MXene.

3.2 Electrochemical characterization for overall water splitting

Electrochemical characterization is of the utmost importance and unique techniques to check the performance of synthesized materials in energy storage applications. The catalytic activity and the reaction mechanisms involved for electron transfer, mass transport, charge transfer, electrolyte transport are also examined by electrochemical techniques. To investigate the catalytic performance of the synthesized materials for overall water splitting, hydrogen evolution reactions (HER) and oxygen

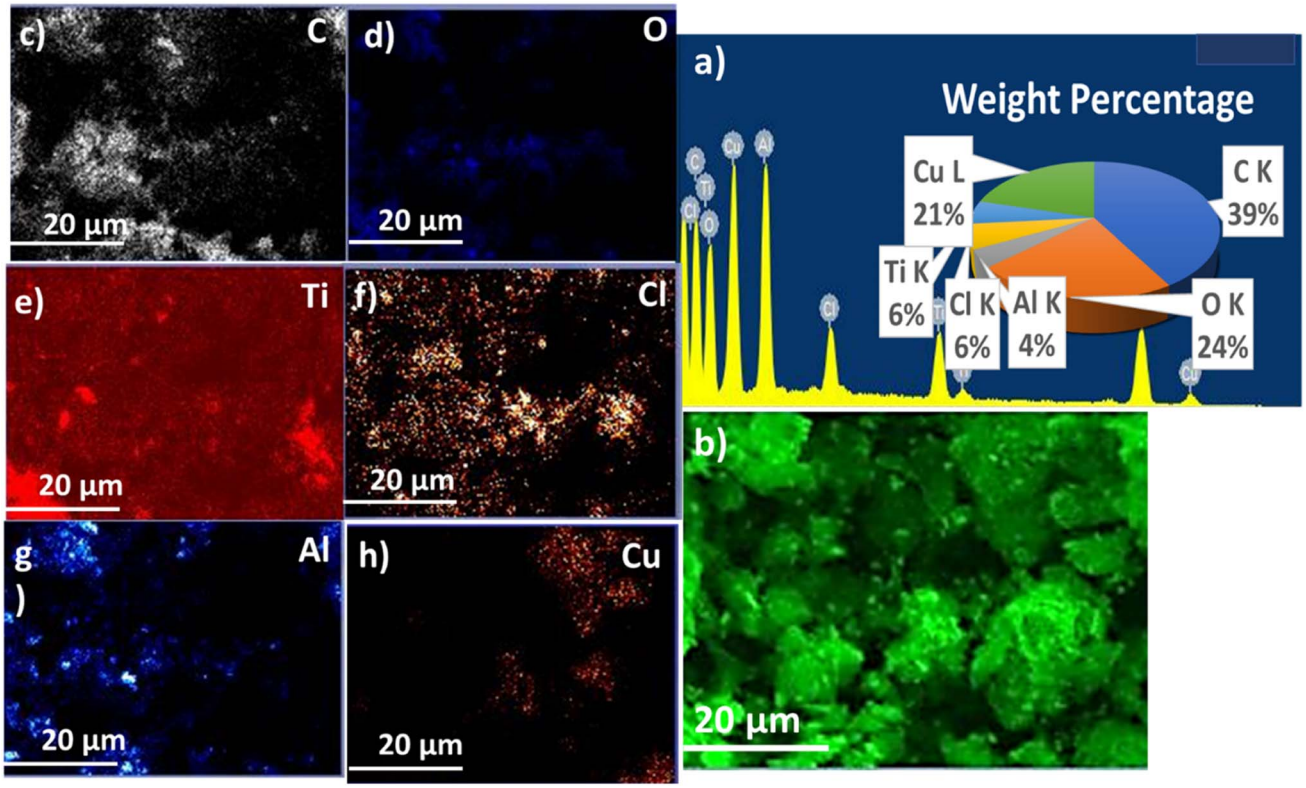

Fig. 3 (a) and (b) EDX analysis of Cl-terminated MXene with weight percentage of all elements present in Cl-terminated MXene, (c)–(h) elemental mapping of all the present elements in synthesized Cl-terminated MXene.

evolution reactions (OER) was performed along with the cyclovoltammetry (CV) and chronopotentiometry (CP) analysis.

All the electrochemical tests were performed out in a three-electrode system with silver/silver chloride (Ag/AgCl) as a reference electrode. Platinum (Pt) mesh was used as a counter electrode while the working electrode was a 1 cm × 1 cm piece of nickel foam on which all three different prepared MXenes (HF-MXene, Cl-terminated MXene, and CuS/Cl-terminated MXene) were deposited. 1 M KOH solution was used as an electrolyte. For HERs, linear sweep voltammetry (LSV) was performed in the potential range of −0.5 V to 0 V (*vs.* RHE). To check the performance of $CuS/Ti_3C_2Cl_2$ compared to other manufactured materials, 10 mA cm^{-2} current density was set as a reference point in the case of HER. Fig. 5(a) shows the enormously improved HER activity of $CuS/Ti_3C_2Cl_2$ as compared to other materials. To deliver the same (10 mA cm^{-2}) amount of

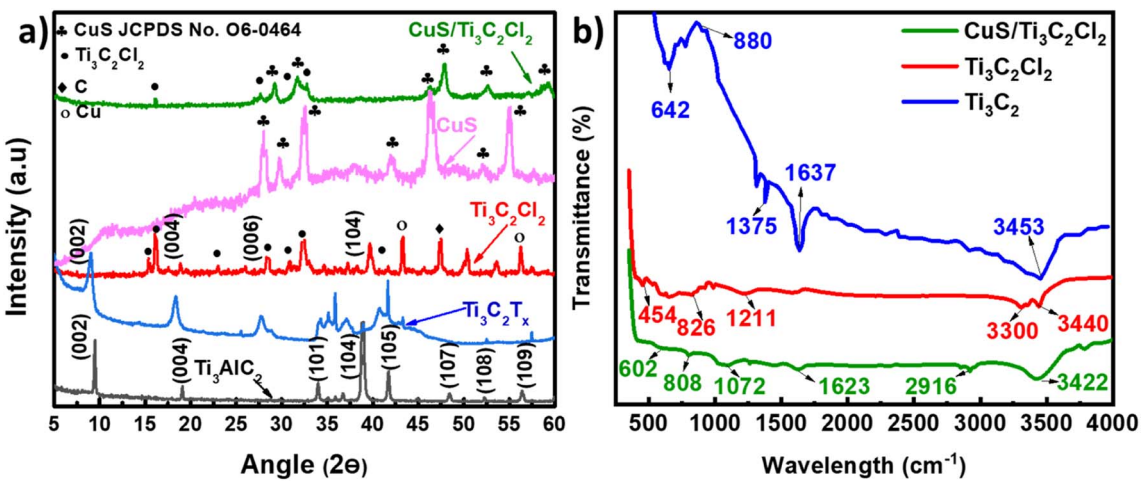

Fig. 4 (a) XRD analysis of MAX phase (Ti_3AlC_2), HF-MXene ($Ti_3C_2T_x$), Cl-MXene ($Ti_3C_2Cl_2$), CuS and composite $CuS/Ti_3C_2Cl_2$, (b) FTIR spectrum of HF-MXene ($Ti_3C_2T_x$), Cl-MXene ($Ti_3C_2Cl_2$) and CuS/Cl-MXene ($CuS/Ti_3C_2Cl_2$).

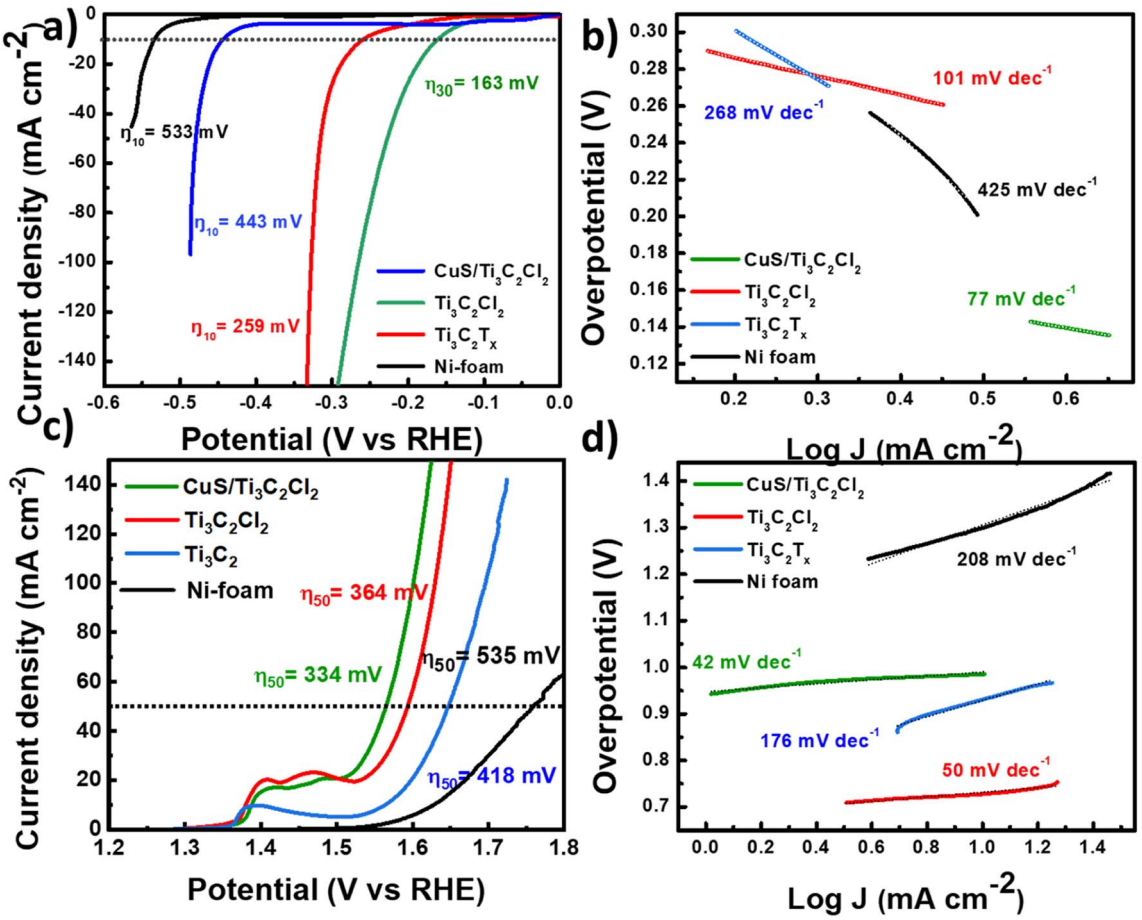

Fig. 5 (a) HER analysis of Ni foam, HF-MXene (Ti_3AlC_2), Cl-MXene ($Ti_3C_2Cl_2$) and CuS/Cl-MXene ($CuS/Ti_3C_2Cl_2$), (b) corresponding HER Tafel slopes of Ni foam, HF-MXene (Ti_3AlC_2), Cl-MXene ($Ti_3C_2Cl_2$) and CuS/Cl-MXene ($CuS/Ti_3C_2Cl_2$), (c) OER behavior of Ni foam, HF-MXene ($Ti_3Al_2C_2$), Cl-MXene ($Ti_3C_2Cl_2$) and CuS/Cl-MXene ($CuS/Ti_3C_2Cl_2$), (d) corresponding OER Tafel slopes.

current density, HF-MXene required a huge overpotential of 443 mV, while Cl-terminated MXene needs 259 mV overpotential to achieve 10 mA cm^{-2} current. As expressed in XRD analysis, the improvement in HER performance was due to the increase in interlayer distance of MXene sheets which aids the intercalation.[45] Another reason is the highly ordered crystalline structure of Cl-terminated MXene synthesized at a higher temperature which leads towards efficient hydrogen evaluation. The ordered structures enable the accurate determination of the preferred sites on Cl-terminated MXene.[46] $CuS/Ti_3C_2Cl_2$ shows an overpotential of 163 mV which is the lowest valve of overpotential among all.[47,48] This is due to the presence of CuS particles between the layers of Cl-terminated MXene. The onset potential values shown by bare Ni foam, HF-MXene, Cl-terminated MXene, and CuS/Cl-terminated MXene are 515 mV, 412 mV, 234 mV, and 124 mV, respectively. To further support enhanced HER activity of $CuS/Ti_3C_2Cl_2$, Tafel slopes of all the synthesized materials were calculated and shown in Fig. 5(b). Fig. 5(b) reveals that $CuS/Ti_3C_2Cl_2$ has a slope of 77 mV dec^{-1} which is much lesser than the slopes of $Ti_3C_2Cl_2$, Ti_3C_2 and bare Ni foam (101 mV dec^{-1}, 268 mV dec^{-1}, 425 mV dec^{-1} respectively).

To explore the other side of water splitting reactions, OER behaviors of all the three manufactured materials were depicted through LSV in Fig. 5(c) from 1.2 V to 1.8 V (*vs.* RHE). The current values of all materials bare Ni foam, HF-MXene (Ti_3C_2), Cl-terminated MXene ($Ti_3C_2Cl_2$), and copper sulfide composite with Cl-terminated MXene ($CuS/Ti_3C_2Cl_2$) increased rapidly after onset potentials of 370 mV, 350 mV, 312 mV, and 287 mV, respectively. As the oxidation peaks of all the prepared materials appeared after 20 mA cm^{-2} current density, so the OER activities of described materials were compared at 50 mA cm^{-2} current density. It is clearly shown in Fig. 5(c) that $CuS/Ti_3C_2Cl_2$ exhibits the least overpotential value of 334 mV among all (364 mV for $Ti_3C_2Cl_2$, 418 mV for Ti_3C_2 and 535 mV for bare Ni foam) to reach a current density of 50 mA cm^2. The reasons behind this improved activity are already mentioned above. For further confirmation for the improved OER activity of $CuS/Ti_3C_2Cl_2$, Tafel slopes were plotted in Fig. 5(d) 42 mV dec^{-1} slope related to $CuS/Ti_3C_2Cl_2$, while 50 mV dec^{-1}, 176 mV dec^{-1}, 208 mV dec^{-1} slopes correspond to $Ti_3C_2Cl_2$ Ti_3C_2, and bare Ni foam respectively.

Fig. 6 shows the CV of individual HF-MXene, Cl-terminated MXene, and copper sulfide/Cl-terminated MXene at different

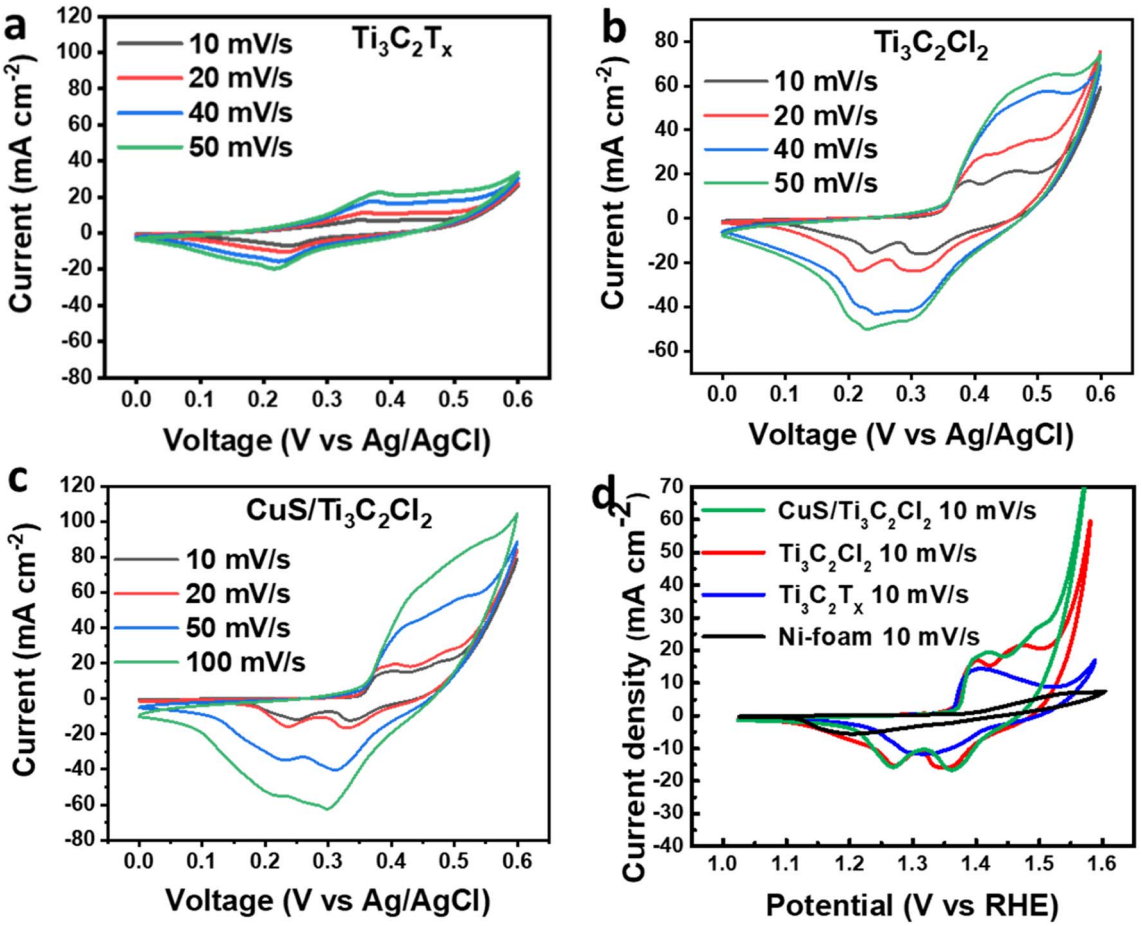

Fig. 6 (a) Cyclovoltammetry (CV) analysis of hydrofluoric acid (HF) based MXene ($Ti_3C_2T_x$) at different scan rates, (b) CV analysis of Cl-terminated MXene ($Ti_3C_2Cl_2$) at different increasing scan rates, (c) CV analysis of CuS/Cl-terminated MXene ($CuS/Ti_3C_2Cl_2$) composite at different scan rates, (d) comparison of CV of Ni foam, HF-MXene, Cl-MXene and CuS/Cl-MXene at 10 mV s^{-1} scan rate.

scan rates, respectively. The CV of all three materials was carried out in the range of 0 to 0.6 V at different scan rates. Redox peaks were examined in the $CuS/Ti_3C_2Cl_2$ cyclic voltammetry (CV) plot demonstrating the reversible faradaic reaction process which may be responsible for changing the oxidation state of Cu.[49] Fig. 6(c) depicts the cyclovoltammetry (CV) of $CuS/Ti_3C_2Cl_2$ in the potential range from 0.9 V to 1.7 (V *vs.* RHE) at different scan rates (10 mV s^{-1} to 100 mV s^{-1}). The redox peaks can be observed at low scan rates. The oxidation peaks at 1.4 V and 1.49 V correspond to nickel foam which is used as a support for catalyst and $CuS/Ti_3C_2Cl_2$ catalyst, respectively.[10] Similarly, the reduction peaks at 1.37 V and is related to nickel foam and synthesized catalyst.[10,50] It shows that increasing the scan rate area under the curves is increasing due to the reduction of diffusion layer resistance, to support higher current density values. The shape of the CV plot did not change much even on higher scan rates, which provide evidence of small resistance, tremendous electrochemical kinetics, and high cyclic stability.[49]

Comparison of cyclovoltammetry (CV) of Ni foam, HF-MXene, Cl-MXene, and CuS/Cl-MXene at 10 mV s^{-1} scan rate in the potential (V *vs.* RHE) range of 1 to 1.6 V as shown in Fig. 6(d). Fig. 6(d) is used to compare the calculated areas under the curve to check the properties. Calculations depicted that CuS/Cl-MXene having more area under the curve than Ni foam (used as substrate), HF-MXene and Cl-MXene respectively.

To check the kinetics of all the prepared materials, EIS analysis was conducted in 1 M KOH solution from the frequency range of 100 mHz to 100 kHz. Fig. 7(a) is the representation of the EIS plot. The equivalent circuit is shown inside a graph in which R_1 shows the ohmic resistance, which is the resistance between the electrodes in an electrolyte. R_2 resistance shows the polarization resistance or the charge transfer resistance. The values of R_1 resistance for CuS/Cl-MXene, Cl-MXene, and HF-MXene are 0.516 Ω, 0.548 Ω, and 2.28 Ω, respectively. Similarly, R_2 values for CuS/Cl-MXene, Cl-MXene, and HF-MXene are 0.219 Ω, 0.348 Ω, 1.96 Ω, correspondingly. The EIS plot on smaller scale shown in Fig. 7(a), clearly depicts that both the ohmic and polarization resistances of CuS/Cl-MXene are lower than other materials because CuS/Cl-MXene has the lowest starting point and shorter width of semicircle as shown in Fig. 7(a). These values provide evidence for the overall minimum resistance of CuS/Cl-MXene among all, indicating enhance electrochemical catalyst activity than single Cl-MXene and ordinary HF-MXene.

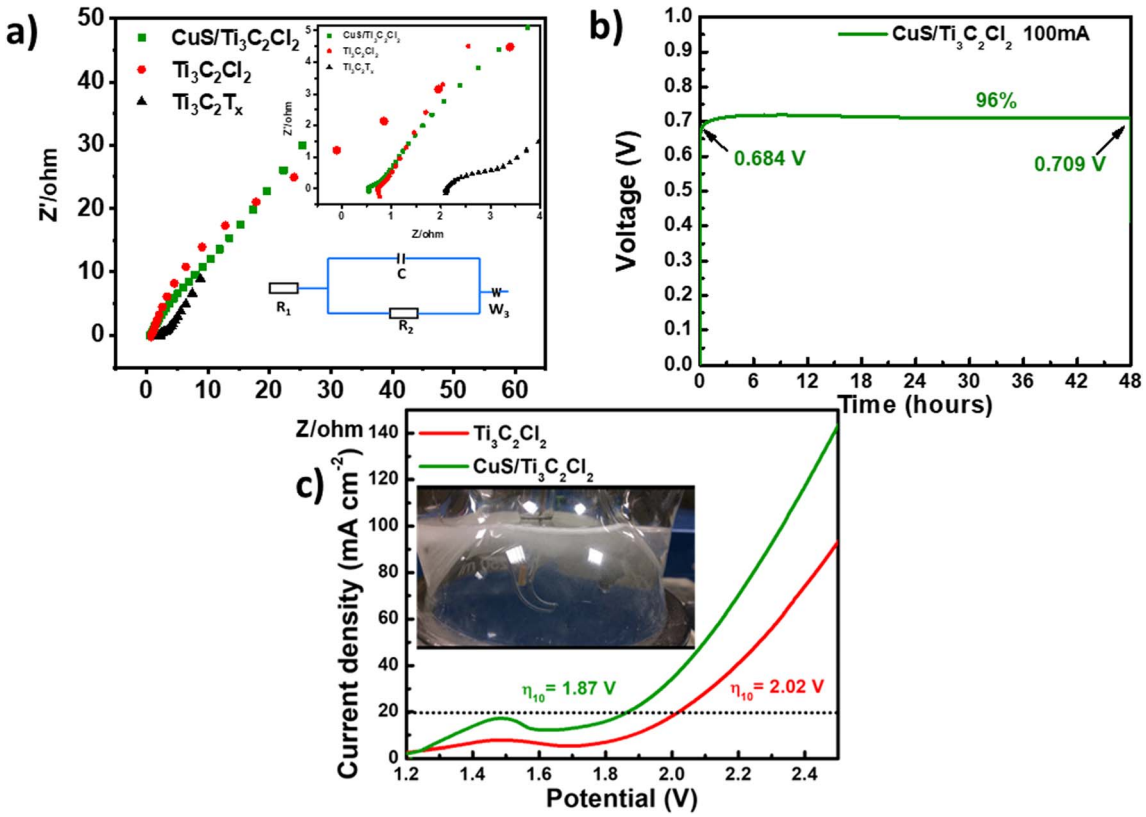

Fig. 7 (a) Electrochemical impedance spectroscopy (EIS) analysis of HF-MXene (Ti_3AlC_2), Cl-MXene ($Ti_3C_2Cl_2$) and CuS/Cl-MXene (CuS/$Ti_3C_2Cl_2$), (b) chronopotentiometry (CP) analysis of synthesized CuS/Cl-MXene (CuS/$Ti_3C_2Cl_2$), (c) overall water splitting curves of both Cl-MXene ($Ti_3C_2Cl_2$) and CuS/Cl-MXene (CuS/$Ti_3C_2Cl_2$).

The chronopotentiometry (CP) analysis for the long-term durability test of synthesized CuS/$Ti_3C_2Cl_2$ electrocatalyst was performed for a cycle of 48 hours at 100 mA cm^{-2} current density is shown in Fig. 7(b). The value of voltage started from 0 V and reached the voltage of 0.684 V in a few minutes, maintained 96% of this value for 48 hours. This stability is achieved by the structural characteristics of synthesized CuS/$Ti_3C_2Cl_2$, due to the activation of the electrocatalyst rapid ion transportation among the active sites is happened and ion diffusion resistance is decreased.

The above investigations reveal that the synthesized CuS/$Ti_3C_2Cl_2$ material can be used as an electrocatalyst for both HER and OER reactions. To further investigate these characteristics overall water splitting test was performed. In 1 M KOH solution, both anode and cathode electrodes were made of CuS/$Ti_3C_2Cl_2$ on nickel foam and tested for overall water splitting as shown in Fig. 7(c). The results of overall water splitting were compared at 20 mA cm^{-2} current density with HF-based MXene. Fig. 7(c) shows that to deliver a current density of 20 mA cm^{-2}, CuS/$Ti_3C_2Cl_2$ exhibit a 1.87 V value of voltage while HF-MXene exhibits a voltage of 2.02 V much higher than CuS/$Ti_3C_2Cl_2$. This value of potential is improved from 2.02 to 1.87 V after the CuS deposition.

Finally, to compare the electrochemical activity for overall water splitting with the reported catalysts, Tables 1 and 2 are prepared. Table 1 shows the hydrogen evolution (HER)

Table 1 HER performance of CuS/Cl-MXene (CuS/$Ti_3C_2Cl_2$) and several reported electrocatalysts

Catalyst	Morphology	Substrate	Electrolyte	Overpotential η (mV)	Current density (mA cm^{-2})	Ref.
(CuS/$Ti_3C_2Cl_2$)	2D sheets	Ni foam	1 M KOH	163	10	This work
CuS	Nano sheets	Ni foam	1 M KOH	279	10	51
$NiSe_2/Ti_3C_2T_x$	2D sheets	Ni foam	2 M KOH	200	10	52
MoS_2/Ni–Al-LDH	Nano sheets	Ni foam	1 M KOH	330	10	48
MoS_2/Ni–Fe-LDH	Nano sheets	Ni foam	1 M KOH	300	10	48
$NiPS_3$	Nano sheets	Ni foam	1 M KOH	530	10	53
MoO_x/Ni_3S_2/Ni foam	Hollow microspheres	Ni foam	1 M KOH	200	15	54
MoS_2@CNF	Nano fibers	Ni foam	1 M KOH	186	10	55

Table 2 OER performance of Cl-terminated MXene ($Ti_3C_2Cl_2$) and several reported electrocatalysts

Catalyst	Morphology	Substrate	Electrolyte	Overpotential η (mV)	Current density (mA cm^{-2})	Ref.
($CuS/Ti_3C_2Cl_2$)	2D sheets	Ni foam	1 M KOH	334	50	This work
Ni–Fe-LDH/MoS_2	Nano sheets	Glassy carbon	1 M KOH	370	50	48
CoNiP/NC-1	Nano strips	Glassy carbon	1 M KOH	330	10	56
$MoCo(OH)_2$/CoP/NF	Nanostructure	Ni foam	1 M KOH	287	10	57
Ni–Al-LDH/MoS_2	Nano sheets	Glassy carbon	1 M KOH	410	50	48
CoP/MXene	Nano sheets	—	1 M KOH	300	50	58
$NiPS_3$	Nano sheets	Glassy carbon	1 M KOH	437	20	59
$NiPS_3$@NiOOH	Nano sheets	RDE	1 M KOH	350	10	60
NiCoS/$Ti_3C_2T_x$	Sheets	Glassy carbon	1 M KOH	365	10	61

performance of our prepared $CuS/Ti_3C_2Cl_2$ with state of the art reported noble metal free catalysts. The data presented in table depicts that the prepared $CuS/Ti_3C_2Cl_2$ electrocatalyst as potential candidate for HER. Similarly, for OER comparison, Table 2 shows prepared $CuS/Ti_3C_2Cl_2$ green electrocatalyst with literature.

4 Conclusion

In summary, the $CuS/Ti_3C_2Cl_2$ bifunctional composite was successfully synthesized by a hydrothermal process. CuS nanoparticles were effectively deposited on the Cl-terminated MXene and significantly increased the interlayer distance of Cl-terminated MXene. The overall electrochemical activity was improved much as compared to bare Cl-terminated MXene and HF-MXene. The overpotential of $CuS/Ti_3C_2Cl_2$ comes out to be 163 mV for HER, which is much less than overpotentials values of Cl-MXene ($Ti_3C_2Cl_2$) and HF-MXene ($Ti_3C_2T_x$) (259 mV and 443 mV respectively) to deliver a current density of 10 mA cm^{-2}. The subsequent Tafel slopes are 77 mV dec^{-1}, 101 mV dec^{-1} and 268 mV dec^{-1} for $CuS/Ti_3C_2Cl_2$, $Ti_3C_2Cl_2$ and $Ti_3C_2T_x$, respectively. Likewise, in the case of OER, the overpotentials to achieve the same current density of 50 mA cm^{-2} are 334 mV, 364 mV, and 418 mV for $CuS/Ti_3C_2Cl_2$, $Ti_3C_2Cl_2$, and $Ti_3C_2T_x$, respectively. Additionally, $CuS/Ti_3C_2Cl_2$ delivered 20 mA cm^{-2} current density for overall water splitting at 1.87 V. Chronopotentiometry (CP) analysis depicted the stable structure of $CuS/Ti_3C_2Cl_2$ composite, the composite retained 96% of its starting value for 48 hours of long time at specific current density value of 100 mA cm^{-2}. All the above electrochemical investigations indicate that $CuS/Ti_3C_2Cl_2$ its auspicious applications in overall water splitting and high-performance electrochemical storage devices. The excellent electrochemical activities of $CuS/Ti_3C_2Cl_2$ composite also open up the new class of composites with Cl-terminated HF-free greener MXenes for electrochemical energy production and storage applications.

Conflicts of interest

There are no conflicts to declare.

References

1 H. Zhao, L. Liu, R. Vellacheri and Y. Lei, Recent Advances in Designing and Fabricating Self-Supported Nanoelectrodes for Supercapacitors, *Adv. Sci.*, 2017, **4**(10), 1700188, DOI: 10.1002/advs.201700188.
2 P. S. John Miller, Electrochemical Capacitors for Energy Management, *Science*, 2008, **321**(5889), 651–652, DOI: 10.1126/science.1158736.
3 X. Yang, R. Guo, R. Cai, Y. Ouyang, P. Yang and J. Xiao, Engineering high-entropy materials for electrocatalytic water splitting, *Int. J. Hydrogen Energy*, 2022, **47**, 13561–13578, DOI: 10.1016/j.ijhydene.2022.02.123.
4 H. Xu, Y. Zhao, G. He and H. Chen, Race on engineering noble metal single-atom electrocatalysts for water splitting, *Int. J. Hydrogen Energy*, 2022, **47**, 14257–14279, DOI: 10.1016/j.ijhydene.2022.02.152.
5 N. H. Attanayake, A. C. Thenuwara, A. Patra, Y. V. Aulin, T. M. Tran, H. Chakraborty, *et al.*, Effect of Intercalated Metals on the Electrocatalytic Activity of 1T-MoS_2 for the Hydrogen Evolution Reaction, *ACS Energy Lett.*, 2018, **3**(1), 7–13, DOI: 10.1021/acsenergylett.7b00865.
6 H. Zhang, Q. Pan, Z. Sun and C. Cheng, Three-dimensional macroporous W_2C inverse opal arrays for the efficient hydrogen evolution reaction, *Nanoscale*, 2019, **11**(24), 11505–11512, DOI: 10.1039/c9nr03548f.
7 R. Khan, M. T. Mehran, S. R. Naqvi, A. H. Khoja, M. M. Baig, M. A. Akram, *et al.*, A highly efficient A-site deficient perovskite interlaced within two dimensional MXene nanosheets as an active electrocatalyst for hydrogen production, *Int. J. Hydrogen Energy*, 2021, **47**(88), 37476–37489, DOI: 10.1016/j.ijhydene.2021.09.017.
8 S. Hussain, I. Rabani, D. Vikraman, A. Feroze, M. Ali, Y. S. Seo, *et al.*, One-pot synthesis of W_2C/WS_2 hybrid nanostructures for improved hydrogen evolution reactions and supercapacitors, *Nanomaterials*, 2020, **10**, 1–17, DOI: 10.3390/nano10081597.
9 D. Vikraman, S. Hussain, K. Karuppasamy, A. Feroze, A. Kathalingam, A. Sanmugam, *et al.*, Engineering the novel $MoSe_2$-Mo_2C hybrid nanoarray electrodes for energy storage and water splitting applications, *Appl. Catal., B*, 2020, **264**, 118531, DOI: 10.1016/j.apcatb.2019.118531.
10 M. T. Mehran, M. M. Baig, B. Sarfraz, S. R. Naqvi, M. B. Muhammad, *et al.*, 3D hierarchical heterostructured LSTN@NiMn-layered double hydroxide as a bifunctional water splitting electrocatalyst for hydrogen production, *Fuel*, 2021, **285**, 119174, DOI: 10.1016/j.fuel.2020.119174.

11 L. Fan, J. Zhao, X. Luo and Z. Tu, ScienceDirect comparison of the performance and degradation mechanism of PEMFC with Pt/C and Pt black catalyst, *Int. J. Hydrogen Energy*, 2021, **47**, 5418–5428, DOI: **10.1016/j.ijhydene.2021.11.135**.

12 L. H. Karlsson, J. Birch, J. Halim, M. W. Barsoum and P. O. Å. Persson, Atomically Resolved Structural and Chemical Investigation of Single MXene Sheets, *Nano Lett.*, 2015, **15**(8), 4955–4960, DOI: **10.1021/acs.nanolett.5b00737**.

13 I. R. Shein and A. L. Ivanovskii, Graphene-like nanocarbides and nanonitrides of d metals (MXenes): synthesis, properties and simulation, *Micro Nano Lett.*, 2013, **8**, 59–62, DOI: **10.1049/mnl.2012.0797**.

14 V. Nicolosi, M. Chhowalla, M. G. Kanatzidis, M. S. Strano and J. N. Coleman, Liquid exfoliation of layered materials, *Science*, 2013, **331**(6017), 568–571, DOI: **10.1126/science.1226419**.

15 M. Naguib, M. Kurtoglu, V. Presser, J. Lu, J. Niu, M. Heon, *et al.*, Two-dimensional nanocrystals produced by exfoliation of Ti_3AlC_2, *Adv. Mater.*, 2011, **23**, 4248–4253, DOI: **10.1002/adma.201102306**.

16 Q. Tang and Z. Zhou, Graphene-analogous low-dimensional materials, *Prog. Mater. Sci.*, 2013, **58**(8), 1244–1315, DOI: **10.1016/j.pmatsci.2013.04.003**.

17 M. Naguib and Y. Gogotsi, Synthesis of two-dimensional materials by selective extraction, *Acc. Chem. Res.*, 2015, **48**(1), 128–135, DOI: **10.1021/ar500346b**.

18 Q. Tang, Z. Zhou and Z. Chen, Graphene-related nanomaterials: tuning properties by functionalization, *Nanoscale*, 2013, **5**(11), 4541–4583, DOI: **10.1039/c3nr33218g**.

19 P. Sobolčiak, A. Tanvir, K. K. Sadasivuni and I. Krupa, Piezoresistive sensors based on electrospun mats modified by 2D $Ti_3C_2T_x$ MXene, *Sensors*, 2019, **19**(20), 4589, DOI: **10.3390/s19204589**.

20 M. Naguib, V. N. Mochalin, M. W. Barsoum and Y. Gogotsi, 25th anniversary article: MXenes: a new family of two-dimensional materials, *Adv. Mater.*, 2014, **26**, 992–1005, DOI: **10.1002/adma.201304138**.

21 M. Zubair, M. M. Ul Hassan, M. T. Mehran, M. M. Baig, S. Hussain and F. Shahzad, 2D MXenes and their heterostructures for HER, OER and overall water splitting: a review, *Int. J. Hydrogen Energy*, 2022, **47**, 2794–2818, DOI: **10.1016/j.ijhydene.2021.10.248**.

22 O. Mashtalir, M. R. Lukatskaya, M. Q. Zhao, M. W. Barsoum and Y. Gogotsi, Amine-assisted delamination of Nb_2C MXene for Li-ion energy storage devices, *Adv. Mater*, 2015, **27**(23), 3501–3506, DOI: **10.1002/adma.201500604**, This article is licensed under a Creative Commons Attribution-NonCommercial 3.0 Unported Licence.

23 A. Vahidmohammadi, A. Hadjikhani, S. Shahbazmohamadi and M. Beidaghi, Two-Dimensional Vanadium Carbide (MXene) as a High-Capacity Cathode Material for Rechargeable Aluminum Batteries, *ACS Nano*, 2017, **11**(11), 11135–11144, DOI: **10.1021/acsnano.7b05350**.

24 S. Y. Pang, Y. T. Wong, S. Yuan, Y. Liu, M. K. Tsang, Z. Yang, *et al.*, Universal Strategy for HF-Free Facile and Rapid Synthesis of Two-dimensional MXenes as Multifunctional Energy Materials, *J. Am. Chem. Soc.*, 2019, **141**, 9610–9616, DOI: **10.1021/jacs.9b02578**.

25 J. J. R. Kirkpatrick, D. S. Enion and D. A. R. Burd, Hydrofluoric acid burns: a review, *Burns*, 1995, **21**, 483–493, DOI: **10.1016/0305-4179(95)93254-h**.

26 Y. Dong, S. Zheng, J. Qin, X. Zhao, H. Shi, X. Wang, *et al.*, All-MXene-Based Integrated Electrode Constructed by Ti_3C_2 Nanoribbon Framework Host and Nanosheet Interlayer for High-Energy-Density Li-S Batteries, *ACS Nano*, 2018, **12**(3), 2381–2388, DOI: **10.1021/acsnano.7b07672**.

27 C. F. Du, Q. Liang, Y. Zheng, Y. Luo, H. Mao and Q. Yan, Porous MXene Frameworks Support Pyrite Nanodots toward High-Rate Pseudocapacitive Li/Na-Ion Storage, *ACS Appl. Mater. Interfaces*, 2018, **10**, 33779–33784, DOI: **10.1021/acsami.8b13750**.

28 H. Li, Y. Wen, X. Zhu, J. Wang, L. Zhang and B. Sun, Novel Heterostructure of a MXene@NiFe-LDH Nanohybrid with Superior Peroxidase-Like Activity for Sensitive Colorimetric Detection of Glutathione, *ACS Sustainable Chem. Eng.*, 2020, **6**(6), 8019–8028, DOI: **10.1021/acssuschemeng.9b05987**.

29 X. Wang, H. Li, H. Li, S. Lin, W. Ding, X. Zhu, *et al.*, 2D/2D 1T-MoS_2/Ti_3C_2 MXene Heterostructure with Excellent Supercapacitor Performance, *Adv. Funct. Mater.*, 2020, **30**(15), 0190302, DOI: **10.1002/adfm.201910302**.

30 K. Mistry, Jalja, R. Lakhani, B. Tripathi, S. Shinde and P. Chandra, Recent trends in MXene/metal chalcogenides for electro-/photocatalytic hydrogen evolution reactions, *Int. J. Hydrogen Energy*, 2022, **47**(99), 41711–41732, DOI: **10.1016/j.ijhydene.2022.02.049**.

31 J. Lin, F. Tao, L. Wang, L. Chen, Y. Ying, L. Zhang, *et al.*, Solvothermal synthesis of sphere-like CuS microcrystals and improvement as nonenzymatic glucose sensor, *J. Mater. Sci.*, 2013, **48**, 5509–5516, DOI: **10.1007/s10853-013-7345-2**.

32 Y. Wang, X. Zhang, P. Chen, H. Liao and S. Cheng, In situ preparation of CuS cathode with unique stability and high rate performance for lithium ion batteries, *Electrochim. Acta*, 2012, **80**, 264–268, DOI: **10.1016/j.electacta.2012.07.004**.

33 H. Li, Y. Wang, J. Huang, Y. Zhang and J. Zhao, Microwave-assisted Synthesis of CuS/Graphene Composite for Enhanced Lithium Storage Properties, *Electrochim. Acta*, 2017, **225**, 443–451, DOI: **10.1016/j.electacta.2016.12.117**.

34 M. Mousavi-Kamazani, Z. Zarghami and M. Salavati-Niasari, Facile and Novel Chemical Synthesis, Characterization, and Formation Mechanism of Copper Sulfide (Cu_2S, Cu_2S/CuS, CuS) Nanostructures for Increasing the Efficiency of Solar Cells, *J. Phys. Chem. C*, 2016, **120**(4), 2096–2108, DOI: **10.1021/acs.jpcc.5b11566**.

35 X. Zhang, W. Guo and C. Pan, Transparent conducting oxide-free and Pt-free flexible dye-sensitized solar cells employing CuS-nanosheet networks as counter electrodes, *J. Mater. Chem. A*, 2016, **4**(17), 6569–6576, DOI: **10.1039/c6ta01353h**.

36 Z. Pan, F. Cao, X. Hu and X. Ji, A facile method for synthesizing CuS decorated Ti_3C_2 MXene with enhanced

performance for asymmetric supercapacitors, *J. Mater. Chem. A*, 2019, **7**, 8984–8992, DOI: 10.1039/c9ta00085b.

37 M. Li, J. Lu, K. Luo, Y. Li, K. Chang, K. Chen, *et al.*, Element Replacement Approach by Reaction with Lewis Acidic Molten Salts to Synthesize Nanolaminated MAX Phases and MXenes, *J. Am. Chem. Soc.*, 2019, **141**, 4730–4737, DOI: 10.1021/jacs.9b00574.

38 Y. Li, H. Shao, Z. Lin, J. Lu, L. Liu, B. Duployer and Q. Huang, A general Lewis acidic etching route for preparing MXenes with enhanced electrochemical performance in non-aqueous electrolyte, *Nat. Mater.*, 2020, **19**(8), 894–899, DOI: 10.1038/s41563-020-0657-0.

39 F. Liu, A. Zhou, J. Chen, J. Jia, W. Zhou, L. Wang, *et al.*, Preparation of Ti_3C_2 and Ti_2C MXenes by fluoride salts etching and methane adsorptive properties, *Appl. Surf. Sci.*, 2017, **416**, 781–789, DOI: 10.1016/j.apsusc.2017.04.239.

40 J. N. Coleman, M. Lotya, A. O'Neill, S. D. Bergin, P. J. King, U. Khan, K. Young, A. Gaucher, S. De, R. J. Smith and I. V. Shvets, Two-dimensional nanosheets produced by liquid exfoliation of layered materials, *Science*, 2011, **331**(6017), 568–571, DOI: 10.1126/science.1194975.

41 L. Z. Pei, J. F. Wang, X. X. Tao, S. B. Wang, Y. P. Dong, C. G. Fan, *et al.*, Synthesis of CuS and $Cu_{1.1}Fe_{1.1}S_2$ crystals and their electrochemical properties, *Mater. Charact.*, 2011, **62**, 354–359, DOI: 10.1016/j.matchar.2011.01.001.

42 S. Umasankari and R. Anitha, Synthesize and characterization of copper sulfide (CuS) nanoparticle using precipitation method, *Int. J. Adv. Technol. Eng. Sci.*, 2017, **5**, 184–188.

43 M. Saranya, C. Santhosh, R. Ramachandran and A. Nirmala Grace, Growth of CuS nanostructures by hydrothermal route and its optical properties, *J. Nanotechnol.*, 2014, **2014**, DOI: 10.1155/2014/321571.

44 L. Liang, S. Peng, Z. Yuan, C. Wei, Y. He, J. Zheng, *et al.*, Biocompatible tumor-targeting nanocomposites based on CuS for tumor imaging and photothermal therapy, *RSC Adv.*, 2018, **8**, 6013–6026, DOI: 10.1039/c7ra12796k.

45 J. Lu, I. Persson, H. Lind, J. Palisaitis, M. Li, Y. Li, *et al.*, $Ti_{n+1}C_n$ MXenes with fully saturated and thermally stable Cl terminations, *Nanoscale Adv.*, 2019, **1**, 3680–3685, DOI: 10.1039/c9na00324j.

46 W. Sun, S. A. Shah, Y. Chen, Z. Tan, H. Gao, T. Habib, M. Radovic and M. J. Green, Electrochemical etching of Ti_2AlC to Ti_2CT_x (MXene) in low-concentration hydrochloric acid solution, *J. Mater. Chem. A*, 2017, **5**(41), 21663–21668, DOI: 10.1039/C7TA05574A.

47 Y. Wu, G. D. Li, Y. Liu, L. Yang, X. Lian, T. Asefa, *et al.*, Overall Water Splitting Catalyzed Efficiently by an Ultrathin Nanosheet-Built, Hollow Ni_3S_2-Based Electrocatalyst, *Adv. Funct. Mater.*, 2016, **26**, 4839, DOI: 10.1002/adfm.201601315.

48 M. S. Islam, M. Kim, X. Jin, S. M. Oh, N. S. Lee, H. Kim, *et al.*, Bifunctional 2D Superlattice Electrocatalysts of Layered Double Hydroxide-Transition Metal Dichalcogenide Active for Overall Water Splitting, *ACS Energy Lett.*, 2018, **3**, 952–960, DOI: 10.1021/acsenergylett.8b00134.

49 M. Mahmood, I. Hussain, M. Zarrar, M. Taqi and M. Saleem, Electrochimica acta binder-free heterostructured MWCNTs/Al_2S_3 decorated on NiCo foam as highly reversible cathode material for high-performance supercapacitors, *Electrochim. Acta*, 2020, **340**, 135955, DOI: 10.1016/j.electacta.2020.135955.

50 D. S. Liu, D. H. Liu, B. H. Hou, Y. Y. Wang, J. Z. Guo, Q. L. Ning, *et al.*, 1D porous MnO@N-doped carbon nanotubes with improved Li-storage properties as advanced anode material for lithium-ion batteries, *Electrochim. Acta*, 2018, **264**, 292–300, DOI: 10.1016/j.electacta.2018.01.129.

51 G. Shi, Z. Fan, L. Du, X. Fu, C. Dong, W. Xie, *et al.*, In situ construction of graphdiyne/CuS heterostructures for efficient hydrogen evolution reaction, *Mater. Chem. Front.*, 2019, **3**, 821–828, DOI: 10.1039/c9qm00064j.

52 H. Jiang, Z. Wang, Q. Yang, L. Tan, L. Dong and M. Dong, Ultrathin $Ti_3C_2T_x$ (MXene) Nanosheet-Wrapped $NiSe_2$ Octahedral Crystal for Enhanced Supercapacitor Performance and Synergetic Electrocatalytic Water Splitting, *Nano-Micro Lett.*, 2019, **11**, 1–14, DOI: 10.1007/s40820-019-0261-5.

53 C. F. Du, Q. Liang, R. Dangol, J. Zhao, H. Ren, S. Madhavi, *et al.*, Layered Trichalcogenidophosphate: A New Catalyst Family for Water Splitting, *Nano-Micro Lett.*, 2018, **10**, 1–15, DOI: 10.1007/s40820-018-0220-6.

54 Y. Wu, G. D. Li, Y. Liu, L. Yang, X. Lian, T. Asefa, *et al.*, Overall Water Splitting Catalyzed Efficiently by an Ultrathin Nanosheet-Built, Hollow Ni_3S_2-Based Electrocatalyst, *Adv. Funct. Mater.*, 2016, **26**, 4839–4847, DOI: 10.1002/adfm.201601315.

55 M. A. Khan, M. T. Mehran, S. R. Naqvi, A. H. Khoja, F. Shahzad, *et al.*, Reutilizing Methane Reforming Spent Catalysts as Efficient Overall Water-Splitting, *Electrocatalysts*, 2021, **6**(33), 21316–21326, DOI: 10.1021/acsomega.1c01558.

56 D. Chen, J. Luo, Q. Sun and C. Han, Bimetallic phosphide nanoparticles embedded in carbon nanostrips for electrocatalytic water oxidation, *Int. J. Hydrogen Energy*, 2022, **47**(43), 18700–18707, DOI: 10.1016/j.ijhydene.2022.04.036.

57 K. C. Majhi and M. Yadav, Facile hydrothermal synthesis of rare earth phosphate for boosting hydrogen evolution reaction, *Int. J. Hydrogen Energy*, 2022, **47**, 14092–14103, DOI: 10.1016/j.ijhydene.2022.02.168.

58 N. C. S. Selvam, J. Lee, G. H. Choi, M. J. Oh, S. Xu, B. Lim, *et al.*, MXene supported Co: XAy (A = OH, P, Se) electrocatalysts for overall water splitting: unveiling the role of anions in intrinsic activity and stability, *J. Mater. Chem. A*, 2019, **7**, 27383–27393, DOI: 10.1039/c9ta10664b.

59 R. Dangol, Z. Dai, A. Chaturvedi, Y. Zheng, Y. Zhang, K. N. Dinh, *et al.*, Few-layer $NiPS_3$ nanosheets as bifunctional materials for Li-ion storage and oxygen

evolution reaction, *Nanoscale*, 2018, **47**(43), 18700–18707, DOI: **10.1039/c7nr08745d**.

60 B. Konkena, J. Masa, A. J. R. Botz, I. Sinev, W. Xia, J. Koßmann, *et al.*, Metallic $NiPS_3$@NiOOH Core-Shell Heterostructures as Highly Efficient and Stable Electrocatalyst for the Oxygen Evolution Reaction, *ACS Catal.*, 2017, 7(1), 229–237, DOI: **10.1021/acscatal.6b02203**.

61 H. Zou, B. He, P. Kuang, J. Yu and K. Fan, Metal-Organic Framework-Derived Nickel-Cobalt Sulfide on Ultrathin Mxene Nanosheets for Electrocatalytic Oxygen Evolution, *ACS Appl. Mater. Interfaces*, 2018, **10**, 22311–22319, DOI: **10.1021/acsami.8b06272**.